

Multi-task Neural Diffusion Processes

Joseph Rawson¹, Domniki Ladopoulou^{1*}, Petros Dellaportas^{1,2}

^{1*}Department of Statistical Science, University College London, Gower Street, London, WC1E 6BT, United Kingdom.

²Department of Statistics, Athens University of Economics and Business, Patission 76, Athens, 104 34, Greece.

*Corresponding author(s). E-mail(s): domna.ladopoulou.22@ucl.ac.uk;
Contributing authors: p.dellaportas@ucl.ac.uk;

Abstract

Neural diffusion processes provide a scalable, non-Gaussian approach to modelling distributions over functions, but existing formulations are limited to single-task inference and do not capture dependencies across related tasks. In many multi-task regression settings, jointly modelling correlated functions and enabling task-aware conditioning is crucial for improving predictive performance and uncertainty calibration, particularly in low-data regimes. We propose multi-task neural diffusion processes, an extension that incorporates a task encoder to enable task-conditioned probabilistic regression and few-shot adaptation across related functions. The task encoder extracts a low-dimensional representation from context observations and conditions the diffusion model on this representation, allowing information sharing across tasks while preserving input-size agnosticity and the equivariance properties of neural diffusion processes. The resulting framework retains the expressiveness and scalability of neural diffusion processes while enabling efficient transfer to unseen tasks. Empirical results demonstrate improved point prediction accuracy and better-calibrated predictive uncertainty compared to single-task neural diffusion processes and Gaussian process baselines. We validate the approach on real wind farm data appropriate for wind power prediction. In this high-impact application, reliable uncertainty quantification directly supports operational decision-making in wind farm management, illustrating effective few-shot adaptation in a challenging real-world multi-task regression setting.

Keywords: Few-shot inference, uncertainty quantification, probabilistic regression, renewable energy, wind power prediction

1 Introduction

Diffusion probabilistic models have emerged as a powerful approach for learning complex distributions via iterative denoising [1, 2]. Neural diffusion processes (NDPs) are a class of probabilistic models that learn distributions over functions by extending diffusion-based generative modelling to function space [3]. They operate by iteratively corrupting and denoising function values, avoiding explicit Gaussian assumptions while retaining scalability through neural network (NN) parameterisations. In the regression setting, NDPs support uncertainty-aware prediction and allow conditioning on context observations at inference time via conditional inference [3]. These properties make NDPs a flexible foundation for probabilistic regression in complex and non-linear settings.

We introduce multi-task neural diffusion processes (MT-NDPs), an extension of NDPs for regression problems involving collections of related tasks. Many real-world regression settings are inherently multi-task, where functions share common structure while exhibiting task-specific variation, such as multi-sensor measurements [4], spatio-temporal environmental data [5], and wind turbines operating within a wind farm [6–8]. Jointly modelling such tasks improves data efficiency and predictive performance, particularly in low-data regimes [9]. However, existing NDPs are restricted to single-task inference and cannot exploit cross-task correlations, motivating a principled multi-task extension.

Prior work on multi-task probabilistic regression has explored several approaches for sharing information across different tasks. Multi-task Gaussian processes (GPs) provide a Bayesian framework for joint inference via structured cross-task covariance models, including autoregressive formulations that handle incomplete observations across tasks [4, 10, 11]. While effective, these methods scale poorly to large datasets and depend strongly on kernel and covariance design [12]. Neural alternatives such as neural processes (NPs) improve scalability by learning task representations from context sets, and multi-task extensions enable transfer learning across related functions [13–15]. However, these models often suffer from underfitting and inconsistent uncertainty calibration. NDPs address these limitations by learning expressive, non-Gaussian distributions over functions [3], but existing formulations are restricted to single-task inference.

Wind energy systems provide a representative and practically relevant example of multi-task regression, where multiple wind turbines operate under similar environmental conditions while exhibiting turbine-specific behaviour. Accurate and uncertainty-aware wind power prediction is a high-impact application and it is essential for grid stability and maintenance planning, particularly given that operation and maintenance costs account for a substantial fraction of total wind farm expenditure [7, 16]. Prior work has explored a range of probabilistic and machine learning approaches for wind power prediction, including GPs [17–20], quantile regression [21–23], mixture density networks [24], and NN-based probabilistic models [6]. While these methods provide varying degrees of flexibility and uncertainty quantification, many either scale poorly to large datasets or lack principled mechanisms for sharing information across turbines.

To address these challenges, we propose MT-NDPs, which incorporate a task encoder that maps context observations to a low-dimensional task representation and conditions the diffusion denoiser on this representation. This design enables information sharing across related tasks while preserving the set-structured, scalable, and uncertainty-aware properties of NDPs. As a result, MT-NDPs support few-shot adaptation to unseen tasks by conditioning on limited task-specific context at inference time.

We evaluate the proposed framework on wind power prediction from supervisory control and data acquisition (SCADA) data, assessing predictive accuracy, uncertainty calibration, and generalisation to unseen wind turbines under varying context sizes. The results show that MT-NDPs consistently outperform single-task NDPs and GP-based baselines, particularly in regimes with limited task-specific data.

The remainder of the paper is organised as follows. Section 2 introduces NDPs and their core properties. Section 3 presents the proposed multi-task extension. Section 4 describes the dataset and experimental setup, and Section 5 reports the empirical results. Section 6 discusses implications and limitations, and Section 7 concludes.

2 Background: Neural diffusion processes (NDPs)

This section aims to provide an overview of the key concepts used throughout the manuscript. Diffusion probabilistic models learn complex distributions by gradually corrupting data with noise and training a NN to reverse this process [2]. NDPs adapt this framework from finite-dimensional data vectors to function values, enabling probabilistic regression with uncertainty quantification [3]. For completeness, we summarise the diffusion framework in Appendix B. By operating directly in function space, NDPs avoid the restrictive Gaussian assumptions of GPs while retaining scalability through neural architectures. Compared to NPs, NDPs yield better-calibrated predictive distributions and a more consistent treatment of context and target points. On synthetic benchmarks, NDPs have been shown to closely emulate GP behaviour while scaling more effectively to larger datasets [3].

The core idea of NDPs is to replace the fixed finite-dimensional data vector used in standard diffusion models with function evaluations (X, y) . Here $X \in \mathbb{R}^{N \times D}$ is the matrix of input locations and $y \in \mathbb{R}^N$ the corresponding outputs. In the forward process, Gaussian noise is gradually added to the function values y , while the inputs X remain fixed. After T steps, the corrupted outputs resemble white noise. The reverse process is parameterised by a NN that predicts the noise injected at each step, thereby enabling recovery of the original function values.

We now formalise this intuition by introducing the training data representation used by NDPs. Each training instance corresponds to a sampled function $f_i : \mathbb{R}^D \rightarrow \mathbb{R}$ evaluated at a finite set of inputs $x_i \in \mathbb{R}^{N \times D}$ with outputs $y_i = f_i(x_i) \in \mathbb{R}^N$. The overall training dataset is therefore

$$\mathcal{D} = \{(x_i, y_i)\}_{i=1}^M, \quad x_i \in \mathbb{R}^{N \times D}, \quad y_i \in \mathbb{R}^N, \quad (1)$$

where M is the number of sampled functions, N is the number of input locations per function, and D is the input dimension.

Forward process. Let $x_0 = x$ and $y_0 = y$. Then the NDPs gradually add noise following

$$q\left(\begin{bmatrix} x_t \\ y_t \end{bmatrix} \middle| \begin{bmatrix} x_{t-1} \\ y_{t-1} \end{bmatrix}\right) = \mathcal{N}\left(y_t; \sqrt{1 - \beta_t} y_{t-1}, \beta_t I\right) \quad (2)$$

for each timestep t where β_t is the noise from the variance schedule [3]. This forward process is directly analogous to the standard diffusion formulation (Eq. B6 in Appendix B), but adapted to function-space regression by explicitly separating input locations x_t from function values y_t . This corresponds to adding Gaussian noise to the function values y_t while keeping the input locations x_t fixed for all t . By the final timestep ($t = T$), the function values y_t will look like Gaussian noise from $\mathcal{N}(0, 1)$.

Reverse process. The reverse process is parameterised by a NN that predicts the noise injected during the forward diffusion process [2]. The reverse transition is given by [3]:

$$p_\theta\left(\begin{bmatrix} x_{t-1} \\ y_{t-1} \end{bmatrix} \middle| \begin{bmatrix} x_t \\ y_t \end{bmatrix}\right) = \mathcal{N}\left(y_{t-1}; \mu_\theta(x_t, y_t, t), \tilde{\beta}_t I\right) \quad (3)$$

with mean

$$\mu_\theta(x_t, y_t, t) = \frac{1}{\sqrt{\alpha_t}} \left(y_t - \frac{\beta_t}{\sqrt{1 - \alpha_t}} \epsilon_\theta(x_t, y_t, t) \right), \quad (4)$$

where the noise model $\epsilon_\theta : \mathbb{R}^{N \times D} \times \mathbb{R}^N \times \mathbb{R} \rightarrow \mathbb{R}^N$ takes as input the non-corrupted x_t as well as the corrupted y_t , and the timestep t . As in standard diffusion models, $\alpha_t = 1 - \beta_t$ and $\bar{\alpha}_t = \prod_{j=1}^t \alpha_j$.

Training objective. Training proceeds by minimising a denoising score-matching objective,

$$L_\theta = \mathbb{E}_{t, x_0, y_0, \epsilon} \left[\|\epsilon - \epsilon_\theta(x_0, y_t, t)\|^2 \right], \quad (5)$$

where $x_0 = x_t$ for all timesteps t , since the diffusion process is applied only to the outputs while the inputs remain fixed. The corrupted outputs are generated through the following reparameterisation:

$$y_t = \sqrt{\bar{\alpha}_t} y_0 + \sqrt{1 - \bar{\alpha}_t} \epsilon, \quad \epsilon \sim \mathcal{N}(0, I). \quad (6)$$

Unconditional sampling. Given some input locations x , we can sample unconditionally from the trained model prior by starting with random noise and following the reverse process for T timesteps. Specifically, we initialise $y_T \sim \mathcal{N}(0, I)$ and then apply the parametrised kernel for $t = T, \dots, 1$. At each step, the NN predicts the noise added in the forward process, and new noise is reintroduced.

Conditional sampling. One of the main strengths of NDPs, as with NPs, is their ability to quickly adapt with only a small amount of data. Conditional sampling is achieved by reinjecting context points at each timestep, using a slight adaptation of the Repaint algorithm [25]. This guides the reverse process to remain consistent with the context set.

Formally, we are interested in $p(y_0^* | x_0^*, D)$, where $D = (x_0^c \in \mathbb{R}^{M \times D}, y_0^c \in \mathbb{R}^M)$ is the set of context points. The target is initialised as $y_T^* \sim \mathcal{N}(0, I)$. At each timestep, we add noise to the context points, obtaining y_t^c from the forward process. We then take the union of the noisy context points and the input locations $x_0 = \{x_0^*, x_0^c\}$, together with the union of the target outputs and context outputs $y_t = \{y_t^*, y_t^c\}$. Finally, the reverse process kernel samples

$$y_{t-1} \sim \mathcal{N}\left(\frac{1}{\sqrt{\alpha_t}} \left(y_t - \frac{\beta_t}{\sqrt{1 - \alpha_t}} \epsilon_\theta(x_0, y_t, t)\right), \tilde{\beta}_t I\right). \quad (7)$$

Repeating this for $t = T, T - 1, \dots, 1$ means that, at each backward step, the context points steer the process in the desired direction.

2.1 Noise model architecture

The noise model architecture follows [3], designed to generate sensible prior distributions over functions. While any NN could in principle serve as the denoiser, certain structural properties are desirable: There are two key requirements: (i) *Input-size agnosticity*: the model should work for arbitrary numbers of input points N and input dimensions D , producing consistent priors whether inference is carried out at one or many locations. This is achieved by replicating the outputs $y_t \in \mathbb{R}^N$ across D copies so that the network weights do not depend directly on N or D . As a result, one trained NDP can be applied across datasets of varying size and dimensionality. (ii) *Equivariance and invariance*: predictions should not depend on the ordering of inputs, context points, or feature dimensions. Reordering inputs should not change the probability of the data, just as kernels such as the radial basis function (RBF) in GPs are invariant to permutations. To enforce the equivariance and invariance, [3] proposed a bi-dimensional attention block, $A_t : \mathbb{R}^{N \times D \times H} \rightarrow \mathbb{R}^{N \times D \times H}$. This multi-head self-attention mechanism operates jointly across input locations and feature dimensions. Attention weights are computed via dot-product similarity, and multiple heads are run in parallel to capture complementary relationships. This design ensures permutation equivariance and invariance while retaining the flexibility of neural architectures, addressing limitations that are often overlooked in standard NN models.

3 Multi-task neural diffusion processes (MT-NDPs)

We propose a novel architectural addition to extend NDPs to MT-NDPs, borrowing key items from [15]. The broad idea is to add a task encoder that can take context points and use that information to identify the task the model is performing a prediction on. This information is represented in the encoding space by a single vector $v \in \mathbb{R}^\kappa$. That is, the encoding space has dimension κ , allowing enough flexibility for the model to distinguish between different tasks. The dimension κ is assumed to be small; for example, in our experiments described in Section 4, we set $\kappa = 8$. This vector can then be propagated downstream to the diffusion architecture, which remains unchanged. The way we pass the information downstream is simply to concatenate

these extra κ dimensions onto the other input features. These κ additional features will be the same for all points in the same training (or testing) sample.

3.1 Forward Process

Let $x_0 = x$, $y_0 = y$, and suppose we have context points $x^c = x_0^c$, $y^c = y_0^c$, then the MT-NDPs gradually add noise following:

$$q\left(\begin{bmatrix} x_t \\ y_t \\ x_t^c \\ y_t^c \end{bmatrix} \middle| \begin{bmatrix} x_{t-1} \\ y_{t-1} \\ x_{t-1}^c \\ y_{t-1}^c \end{bmatrix}\right) = \mathcal{N}\left(y_t; \sqrt{1 - \beta_t} y_{t-1}, \beta_t I\right) \quad (8)$$

for each timestep t where β_t is the noise from the variance schedule. Notice the similarities to Eq. 2, where now, as well as explicitly differentiating between the input locations x_t and outputs y_t , we also incorporate the context points x_t^c and y_t^c . This corresponds to adding Gaussian noise to the function values y_t while keeping the input locations x_t , and context points (x_t^c, y_t^c) fixed for all t . By the final timestep $t = T$, the function values y_t will look like Gaussian noise from $\mathcal{N}(0, 1)$.

3.2 Reverse Process

MT-NDPs, like NDPs, use an NN that learns to de-noise the corrupted function values, where we now also make use of some context points (x_t^c, y_t^c) . The input locations x_t and context points (x_t^c, y_t^c) are not corrupted, while the y_t are. In fact, the model will use the uncorrupted x_t and (x_t^c, y_t^c) to help improve the de-noising model. The parametrised kernel is of the form:

$$p_\theta\left(\begin{bmatrix} x_{t-1} \\ y_{t-1} \\ x_{t-1}^c \\ y_{t-1}^c \end{bmatrix} \middle| \begin{bmatrix} x_t \\ y_t \\ x_t^c \\ y_t^c \end{bmatrix}\right) = \mathcal{N}\left(y_{t-1}; \mu_\theta(x_t, y_t, x_t^c, y_t^c, t), \tilde{\beta}_t I\right) \quad (9)$$

with

$$\mu_\theta(x_t, y_t, x_t^c, y_t^c, t) = \frac{1}{\sqrt{\alpha_t}} \left(y_t - \frac{\beta_t}{\sqrt{1 - \alpha_t}} \epsilon_\theta^{MT}(x_t, y_t, x_t^c, y_t^c, t) \right), \quad (10)$$

where the noise model $\epsilon_\theta^{MT} : \mathbb{R}^{(N+M) \times D} \times \mathbb{R}^{(N+M)} \times \mathbb{R} \rightarrow \mathbb{R}^N$, now leverages the input locations x_t and context points (x_t^c, y_t^c) . This model is in fact the composition of the encoder model $\epsilon_\theta^{\text{encoder}}$ and the original NDP de-noising model ϵ_θ^{NDP} ,

$$\epsilon_\theta^{MT}(x_t, y_t, x_t^c, y_t^c, t) = \epsilon_\theta^{NDP} \circ \epsilon_\theta^{\text{encoder}}(x_t, y_t, x_t^c, y_t^c, t). \quad (11)$$

This encoder $\epsilon_\theta^{\text{encoder}}(x_t, y_t, x_t^c, y_t^c, t)$ does the following:

- (i) Acts as the identity on (x_t, y_t) , and mapping the (x_t, y_t) to some κ -dimensional space: $\mathbb{R}^{(N+M) \times D} \times \mathbb{R}^{(N+M)} \times \mathbb{R} \rightarrow \mathbb{R}^{N \times D} \times \mathbb{R}^N \times \mathbb{R}^{\kappa \times M}$,
- (ii) Taking the mean over the image of all context points in this κ -dimensional space, $\bar{v} \in \mathbb{R}^\kappa : \mathbb{R}^{N \times D} \times \mathbb{R}^N \times \mathbb{R}^{\kappa \times M} \rightarrow \mathbb{R}^{N \times D} \times \mathbb{R}^N \times \mathbb{R}^\kappa$,

- (iii) Copying this mean vector, \bar{v} , N times so that it can be concatenated with the other input features: $\mathbb{R}^{N \times D} \times \mathbb{R}^N \times \mathbb{R}^\kappa \rightarrow \mathbb{R}^{N \times D} \times \mathbb{R}^N \times \mathbb{R}^{\kappa \times N} = \mathbb{R}^{N \times (D+\kappa)} \times \mathbb{R}^N$

Therefore, given the initial input locations and targets $T = (x_0 \in \mathbb{R}^{N \times D}, y_0 \in \mathbb{R}^N)$ and context points $C = (x_0^c \in \mathbb{R}^{M \times D}, y_0^c \in \mathbb{R}^M)$, after the encoder we preserve T and are left with N copies of a vector $\bar{v} \in \mathbb{R}^\kappa$ that we concatenate to the other input features of x_0 to leave us with $D + \kappa$ dimensional input features, and a modified set of input locations and targets: $T^* = (x_0^* \in \mathbb{R}^{N \times (D+\kappa)}, y_0^* \in \mathbb{R}^N)$ that is then passed through the NDP de-noising model $\epsilon_\theta^{NDP}(x_t^*, y_t^*, t) : \mathbb{R}^{N \times (D+\kappa)} \times \mathbb{R}^N \rightarrow \mathbb{R}^N$. By constructing the task encoder in this way, we ensure agnosticity to input size. Permutation invariance with respect to the ordering of context points is ensured by aggregating context information through the mean operator $\bar{v} \in \mathbb{R}^\kappa$. The target points are kept unchanged by the encoder. This construction is compatible with invariant noise model architectures, as discussed in Section 2.1.

3.3 Objective

The objective is very similar to the NDP objective in Eq. 5:

$$L_\theta = \mathbb{E}_{t, x_0, y_0, x_0^c, y_0^c, \epsilon} \left[\left\| \epsilon - \epsilon_\theta^{MT}(x_0, y_t, x_0^c, y_0^c, t) \right\|^2 \right], \quad (12)$$

where $x_0 = x_t$, $x_0^c = x_t^c$, and $y_0^c = y_t^c$ for all timesteps t and y_t follows the same corruption process as in Eq. 6.

3.4 Sampling

Unconditional sampling remains unchanged from the NDP setup described in Section 2, as we use no context points at all. Simply take $y_T \sim \mathcal{N}(0, I)$, and then for $t = T, \dots, 1$ apply the parametrised kernel. For conditional sampling, we still follow the process for conditional sampling of NDPs described in Section 2, but now using our upgraded de-noising model ϵ_θ^{MT} :

$$y_{t-1} \sim \mathcal{N} \left(\frac{1}{\sqrt{\alpha_t}} \left(y_t - \frac{\beta_t}{\sqrt{1 - \bar{\alpha}_t}} \epsilon_\theta^{MT}(x_0, y_t, x_0^c, y_0^c, t) \right), \tilde{\beta}_t I \right). \quad (13)$$

Note that we still benefit from the Repaint algorithm as we iterate through the reverse process for $t = T, \dots, 1$.

4 Experiments

Wind farm SCADA data provide a realistic and challenging benchmark for multi-task probabilistic regression. The data are high-frequency, noisy, and high-dimensional, and wind farms consist of multiple turbines that operate under broadly similar environmental conditions while exhibiting turbine-specific behaviour. This setting naturally motivates models that can share information across turbines while adapting to individual dynamics. From a modelling perspective, this application places simultaneous demands on scalability, uncertainty calibration, and cross-task generalisation. Models

must handle large datasets spanning multiple years, provide reliable predictive uncertainty, and adapt to turbines with limited historical data. In particular, the ability to condition predictions on a small number of turbine-specific observations at inference time is essential in realistic operational scenarios. These properties make wind farm SCADA data well-suited for evaluating MT-NDPs. In the following experiments, we evaluate model performance in terms of predictive accuracy, uncertainty calibration, and generalisation to unseen turbines under varying numbers of context points.

Dataset. We use SCADA data from the six Senvion MM92 wind turbines at Kelmash wind farm in the UK [26]. The dataset spans January 2016 to July 2021 at a ten-minute resolution, comprising more than 1.7 million records across 110 variables, including wind speed, wind direction, power output, and component temperatures. Each variable is reported as mean, minimum, maximum, and standard deviation within the ten-minute bins. Further details on SCADA variables and the complete data cleaning procedure are provided in the Appendix C. All preprocessing steps are applied consistently across models.

Baselines. We compare the proposed MT-NDP framework with single-task NDP (ST-NDP) baselines trained independently per wind turbine. All NDP variants share the same diffusion architecture, differing only in whether task-specific information is incorporated. To assess the effect of input dimensionality, ST-NDP models are evaluated using both one-dimensional and five-dimensional feature sets. We additionally compare against GP baselines as a classical probabilistic regression approach. While GPs provide principled uncertainty estimates in small-data regimes, they scale poorly with dataset size and dimensionality, and sparse approximations have been shown to yield underconfident uncertainty estimates on this dataset [6]. GP models are trained per turbine using the same data splits and preprocessing as the NDP-based models. Theoretical background and further details for the GP baselines are provided in Appendix A.

4.1 Training and testing framework

Some aspects of the experimental design are common to all comparisons and are therefore outlined here. NDPs learn distributions over functions, which requires training on many function samples. In our setting, each function sample consists of 100 covariate–target pairs. To reduce the impact of autocorrelation in wind generation, both training and testing samples are shuffled so that they are not sequential. For these samples to represent meaningful draws from the underlying stochastic process, all points in a given sample are taken from the same turbine.

To evaluate the ability of NDPs to generalise, we train models on turbines 2–6 and test them on turbine 1. Context points, drawn from the training split of turbine 1, are provided during inference to guide predictions. This setup allows us to assess (i) how informative the learned prior is in the absence of context points, and (ii) the benefit of incorporating context points for accuracy and uncertainty calibration.

All features are standardised per wind turbine, using the mean and standard deviation from the wind turbine’s training set. This step is necessary for both NDPs and

GPs. To ensure fair comparisons, we use the same test functions across all models and context sizes. Context sets of size 0, 25, and 50 points are considered. During training, the number of context points in each set is sampled uniformly from the integers 0 to 50. This setting exposes the model to situations with no context, with few context points, and with many context points. As a result, the model learns both a global prior when no context is provided and task-specific priors when context points are available. This design reflects realistic deployment scenarios, where the amount of available historical data can vary substantially across turbines. Each evaluation uses 30 test functions of length 100.

4.2 Model parameters

For all NDP variants, we use a cosine noise schedule [27] with $T = 500$ diffusion steps. The denoising NN has 4 hidden layers of dimension 64, with multi-head self-attention using $\kappa = 8$ heads. The optimiser is ADAM [28], following the configuration of [3], with a 20-epoch warmup, 200-epoch decay, learning rate schedule ($2 \times 10^{-5} \rightarrow 10^{-3} \rightarrow 10^{-5}$), and an EMA weight of 0.995. For sampling, we generate 200 reverse diffusion trajectories in the one-dimensional case and 100 in higher-dimensional settings, balancing predictive sharpness with computational cost.

In the multi-task framework, the task encoder is an MLP with 4 layers of size 64, GeLU activations, and an 8-dimensional output embedding. The mean embedding across all context points forms a task representation vector. Training is performed for 250 epochs using batches of 32 function samples of length 100, with 500 samples drawn per wind turbine (5 tasks/turbines in total), and 100 randomly shuffled function samples presented per epoch.

Note that the MLP-based encoder does not guarantee invariance to permutations of input features. Enforcing full invariance would require multi-head self-attention blocks, as used in the NDP noise model described in Section 2.1, but would substantially increase model complexity and computational cost. In the wind farm setting, where the ordering of input features can be fixed across training and testing, the lack of invariance is less problematic than it would be in broader meta-learning settings.

4.3 Model evaluation

We evaluated both point accuracy and predictive uncertainty. Results are averaged over 30 test function samples, each containing 100 input–output pairs, and over the specified numbers of context points $C \in \{0, 25, 50\}$.

For a given test sample s , let $\{(x_i, y_i)\}_{i=1}^N$ with $N = 100$ denote inputs and ground-truth outputs; \hat{y}_i is the model’s point prediction. For NDP/MT-NDP models, point predictions are the empirical mean over reverse-diffusion trajectories at each x_i , and central prediction intervals are the corresponding empirical quantiles across trajectories. We report summary statistics in Tables 1 and D1, obtained by averaging per-sample metrics over 30 test samples, each with $N = 100$ input–output pairs, for each (model \times context size) configuration.

To assess point prediction accuracy, we compute the following per-sample losses for each test set: (i) mean absolute error (MAE), defined as $\text{MAEs} = \frac{1}{N} \sum_{i=1}^N |y_i - \hat{y}_i|$ and (ii) root mean squared error (RMSE), defined as $\text{RMSEs} = \sqrt{\frac{1}{N} \sum_{i=1}^N (y_i - \hat{y}_i)^2}$.

To evaluate predictive uncertainty, we compute the coverage error (CE), which quantifies the discrepancy between the nominal coverage q and the actual coverage achieved by the predictive intervals:

$$CE_s = \frac{1}{|Q|} \sum_{q \in Q} \left| \frac{1}{n_s} \sum_{i=1}^{n_s} \mathbf{1}\{y_i^{(s)} \in I_q^{(s)}(x_i)\} - q \right|, \quad (14)$$

where Q is the set of nominal quantile levels and $q \in Q$ denotes a particular level, $y_i^{(s)}$ and n_s denote the observed outputs and number of points respectively in sample s , and the term $I_q^{(s)}(x_i)$ is the predicted interval at coverage level q for that input. The indicator function $\mathbf{1}\{\cdot\}$ equals 1 if the condition inside holds and 0 otherwise. The inner average computes the empirical coverage at level q , subtracting q gives the deviation from the nominal level, and the absolute value penalises both under- and over-coverage equally. Averaging across all $q \in Q$ yields the mean coverage error CE_s , with smaller values indicating better calibrated predictive intervals. Hence, a good model yields $CE_s \approx 0$, indicating predictive intervals that closely align with their nominal coverage.

4.4 Illustrative examples

We provide qualitative illustrations of the diffusion dynamics underlying NDPs, complementing the theoretical framework presented in Section 2. The aim is to build intuition for the forward corruption process and for the behaviour of unconditional and conditional sampling during reverse diffusion. We focus on a one-dimensional regression setting for clarity and visualise representative trajectories at different diffusion timesteps. Fig. 1 illustrates the forward diffusion process, where Gaussian noise is gradually added to the outputs using a cosine variance schedule [27]. As the timestep t increases, the data loses structure and converges towards white noise. This process is applied independently at each input location while the inputs themselves remain fixed.

Unconditional sampling starts from random noise and follows the reverse diffusion process for a fixed number of timesteps. Even without any context information, the resulting samples already resemble the overall data distribution, indicating that the learned prior captures meaningful structure. For wind turbine data, where the relationships between inputs and power output are similar across turbines, the prior alone often produces plausible results.

Conditional sampling incorporates context points at each timestep of the reverse process, guiding the trajectories towards functions that are consistent with the observed data. Initially, when y_t^* is close to pure noise, the context points already contain useful structure. This pulls the reverse trajectories towards functions consistent with the context set, leading to samples that better fit the true data. Fig. 2 compares unconditional and conditional sampling. Even at early timesteps, the conditional trajectories are visibly influenced by the context points, producing outputs that more

closely match the true data throughout the reverse process. To illustrate the dynam-

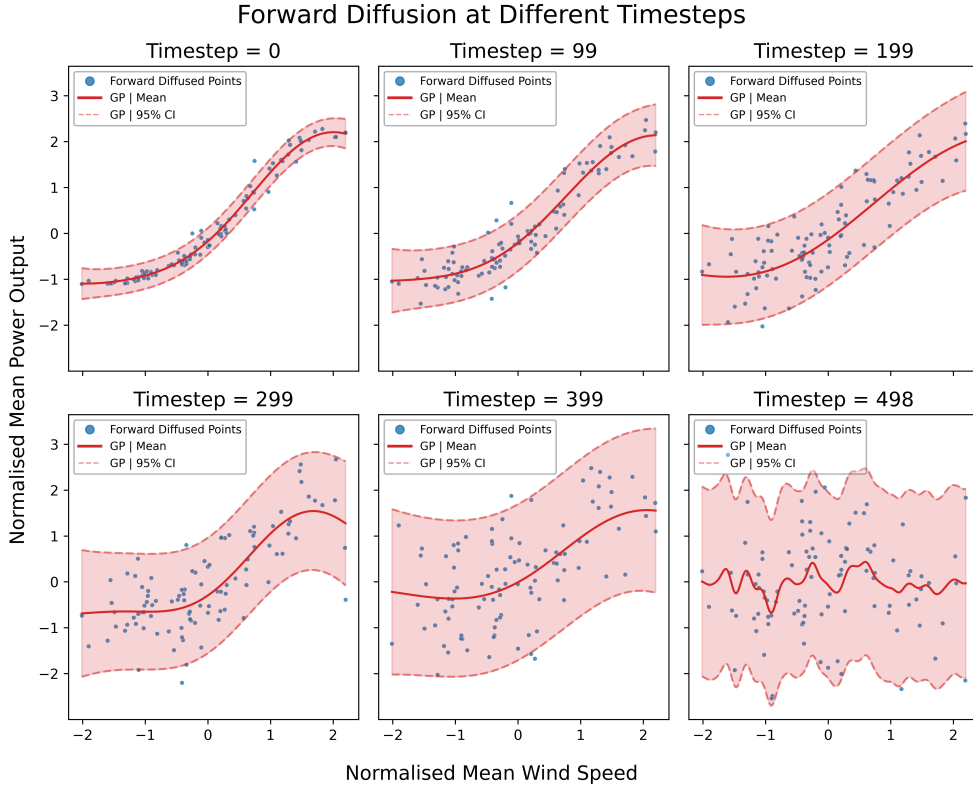


Fig. 1: Illustration of the forward diffusion process. Gaussian noise is added incrementally at each timestep under a cosine variance schedule, progressively degrading the structure of the data until it converges to white noise. GP: Gaussian process, CI: Confidence interval.

ics more clearly, Fig. 3 depicts the forward and reverse trajectories for a single input point. In the forward process (blue), Gaussian noise gradually corrupts the true value. In the reverse process (red), starting from pure noise, the trajectories converge back to the true value, while uncertainty narrows as the timestep t decreases.

5 Results

We first compare a one-dimensional GP with a one-dimensional NDP, using only wind speed as a feature. In this setting, wind turbines are nearly indistinguishable, consistent with exploratory analysis (Appendix, Fig. C1a). For the GP, we mimic the NDP setup, training on turbines 2–6 and testing on turbine 1. Due to scalability limits, the GP is trained on a subsample of 2000 points evenly drawn from the five turbines. We compare this GP baseline only to the NDP with no context points, ensuring a fair assessment of prior quality.

Conditional vs Unconditional Backward Diffusion (GP Smoothed)

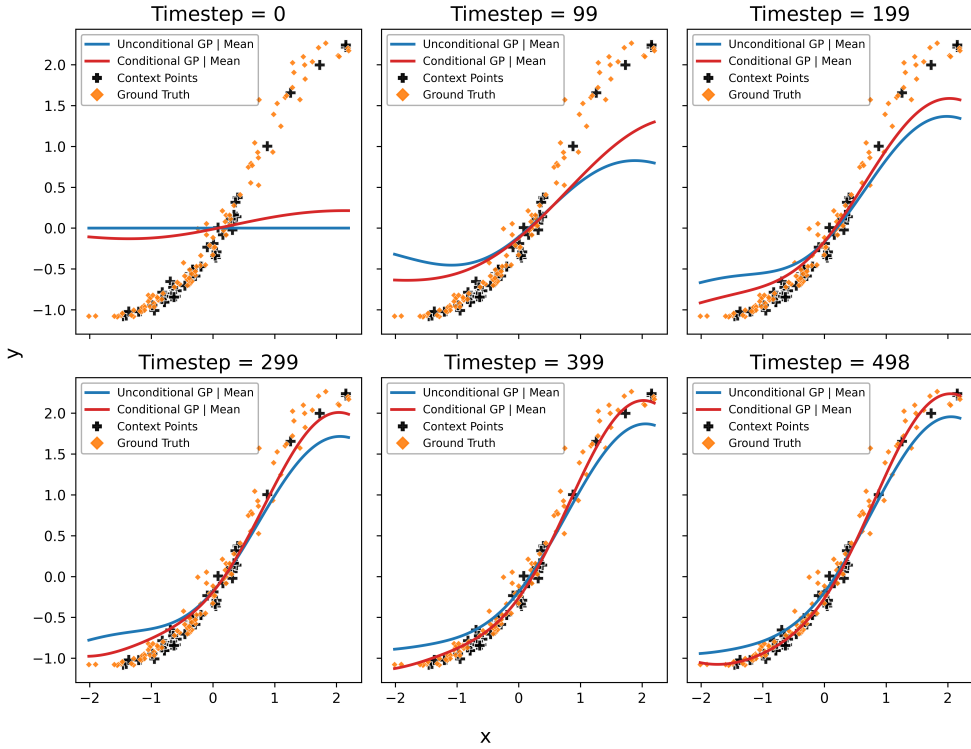


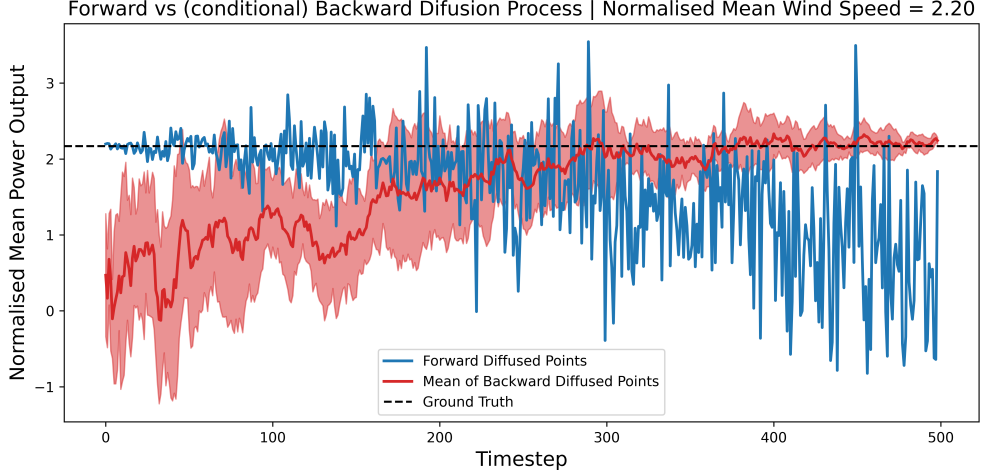
Fig. 2: Comparison of unconditional and conditional reverse diffusion sampling. We sampled 10 reverse trajectories per input location, plotting the mean of these. Conditional sampling provides a closer fit to the true data across all timesteps. GP: Gaussian process.

This comparison indicates that NDPs can be competitive with GPs on this dataset, motivating their use as a foundation for more expressive models. We then investigate the effect of increasing input dimensionality by comparing one-dimensional and five-dimensional NDPs. The higher-dimensional model additionally incorporates wind direction (encoded via sine and cosine components), nacelle temperature, and transformer temperature. These variables were selected based on exploratory analysis (Fig. C2), which revealed strong and nonlinear relationships with power output. For conciseness, the detailed results for this comparison are reported in the Appendix D.

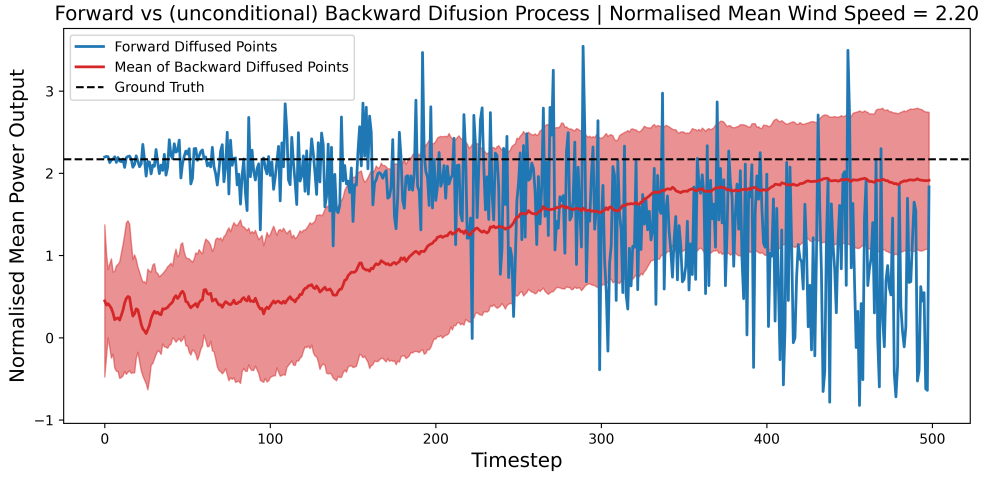
Finally, we assess the benefits of extending NDPs to the multi-task setting. We evaluate two variants, one single-task NDP with five input features and no task encoder, and our multi-task NDP using both encoder and conditional diffusion with Repaint.

5.1 GP against NDP

We first compare the one-dimensional NDP without context points against a GP baseline. The effect of context on NDP performance is examined separately in Sections



(a) conditional sampling



(b) unconditional sampling

Fig. 3: Forward and backward trajectories for a single input point (a) conditional sampling and (b) unconditional sampling. For both (a) and (b) in the forward process (blue), Gaussian noise is gradually added. In the reverse process (red), noise is removed, converging towards the true value with decreasing uncertainty. The shaded area shows one standard deviation.

5.2 and Appendix Section D. Fig. 4 shows the fit of both models on a representative test function of 100 points from turbine 1. While both capture the mean trend well, their uncertainty estimates differ substantially. The NDP derives uncertainty from quantiles of reverse-diffusion trajectories, without assuming Gaussianity, whereas the GP relies on Gaussian predictive distributions. As a result, the GP is clearly underconfident, even in dense regions ($x \in [-1, 1]$). This discrepancy becomes more pronounced in

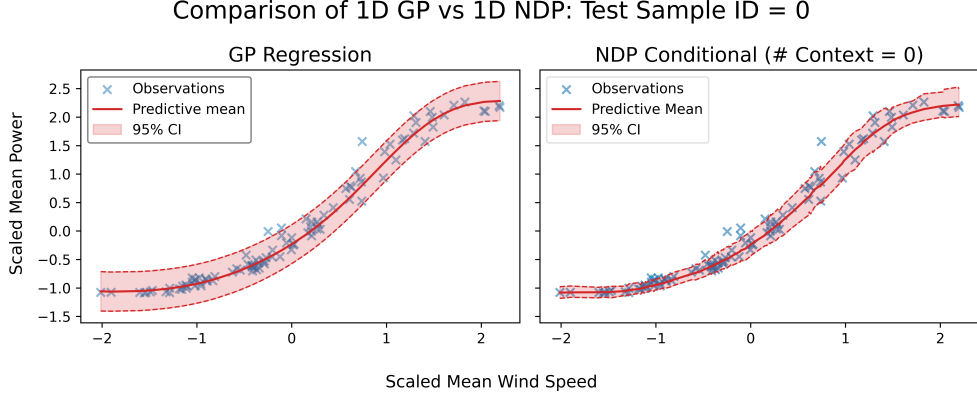
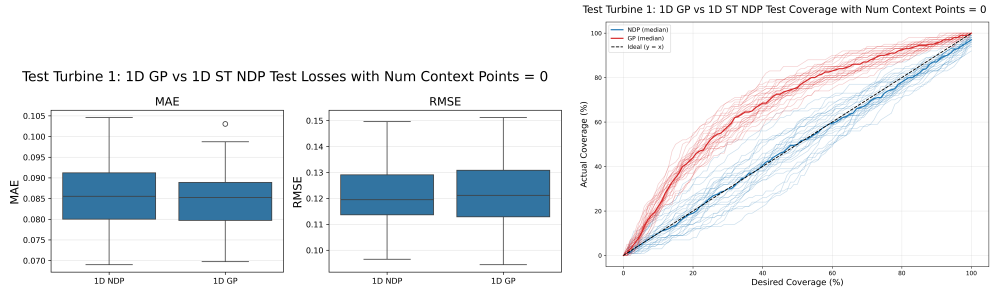


Fig. 4: Fit of Gaussian process (GP) (left) and neural diffusion process (NDP) (right) on a test sample of 100 points from turbine 1, with 95% confidence intervals (CI) on normalised wind speed and power output. 1D: One-dimensional.

extrapolation regions ($x < -1$), where the NDP produces appropriately narrower confidence intervals. At the upper end of the domain ($x > 1$), improvements are less marked, though the NDP still provides slightly tighter uncertainty bounds than the GP.



(a) Mean absolute error (MAE, left) and root mean square error (RMSE, right) distributions for Gaussian process (GP) and neural diffusion process (NDP) over 30 test samples, each with 100 points. (b) Observed vs. theoretical coverage probabilities for Gaussian process (GP) and neural diffusion process (NDP) over 30 test samples, each with 100 points.

Fig. 5: Comparison of Gaussian process (GP) and neural diffusion process (NDP) on turbine 1 test data. (a) Point prediction accuracy (MAE and RMSE distributions). (b) Predictive uncertainty calibration (coverage probabilities). 1D: One-dimensional, ST: single-task

Considering all 30 test samples of 100 points each, both models achieve comparable point prediction accuracy. As shown in Fig. 5a, the distributions of MAE and RMSE for the GP and NDP are nearly indistinguishable, indicating that both capture the mean power–wind speed relationship effectively. The distinction between the models becomes clear when evaluating predictive uncertainty. Fig. 5b shows the empirical coverage against the nominal coverage level. A perfectly calibrated model would follow

the diagonal $y = x$ line. While the NDP is not flawless, it consistently lies closer to this ideal than the GP, which suffers from pronounced underconfidence across coverage levels. This highlights a key strength of NDPs: the ability to generate well-calibrated uncertainty estimates without relying on Gaussian assumptions.

5.2 NDP against MT-NDP

5.2.1 Encoder analysis

To understand how the encoder represents turbines, we project its κ -dimensional embeddings into two principal components using principal component analysis (PCA). Fig. 6 shows the resulting clusters when the model is trained on turbines 2–6 and tested on turbine 1, with context set sizes ranging from very small (0–4 points) to large (46–50 points). With few context points (left panel), wind turbines are essentially indistinguishable, reflecting the fact that the model has little task-specific information and must rely on its global prior. As context increases (middle and right panels), the encoder begins to separate turbines, with turbine 6 in particular forming a clearly distinct cluster. By contrast, turbine 1 remains centred near the origin across all context sizes.

PC Projection of Encoder Embeddings by Turbine Across Context Sizes (Trained on Turbines 2-6)

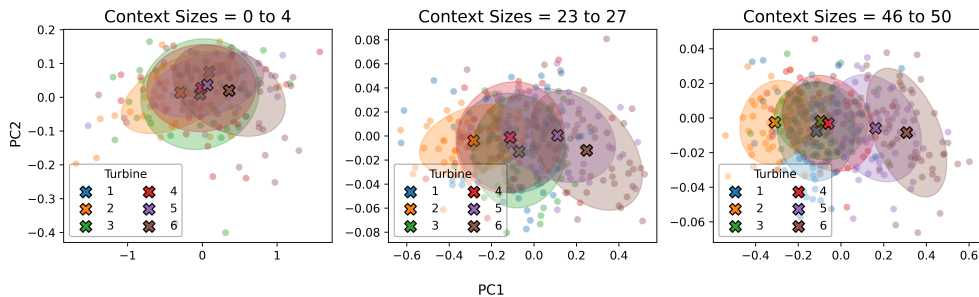


Fig. 6: Principal component (PC) projection of encoder embeddings for turbines 1–6, trained on turbines 2–6. Each panel corresponds to a different range of context set sizes. Colours denote turbines, shaded ellipses show 68% coverage regions, and crosses mark cluster means. As context increases, the encoder begins to separate turbines, with turbine 6 emerging as the most distinct.

These findings have two key implications for evaluation. First, turbine 1 is not an informative test case for the MT-NDP, as its embeddings remain close to the global prior, and additional context yields little task-specific adaptation. Second, turbine 6 emerges as the most distinctive and challenging turbine in the wind farm, requiring the model to rely strongly on context information. For this reason, we focus our quantitative evaluation on turbine 6 in the following sections, as it provides a more discriminative test of the MT-NDP’s ability to adapt beyond the global prior.

5.2.2 Model comparison

Fig. 7 reports the point prediction errors (MAE and RMSE) for three models: the one-dimensional ST-NDP, the five-dimensional ST-NDP, and the five-dimensional MT-NDP. All models improve with increasing context size, but the gains are most pronounced for the five-dimensional MT-NDP, which consistently achieves the lowest errors when 25 or 50 context points are available. This highlights the value of the task encoder in leveraging limited context to improve predictions on unseen wind turbines.

Test Turbine 6: NDP Test Losses by Model and Number of Context Points

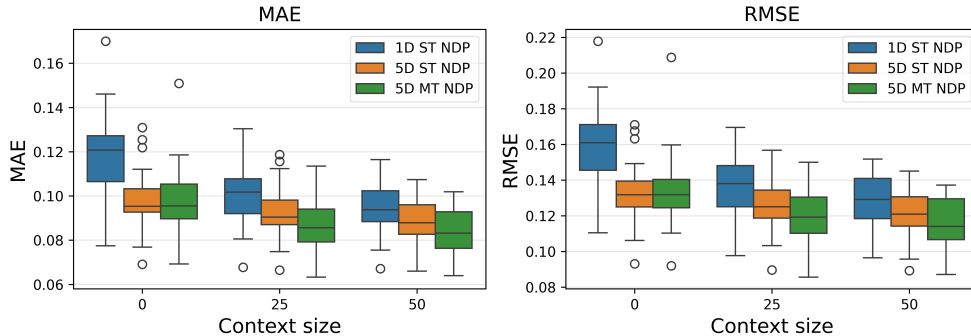
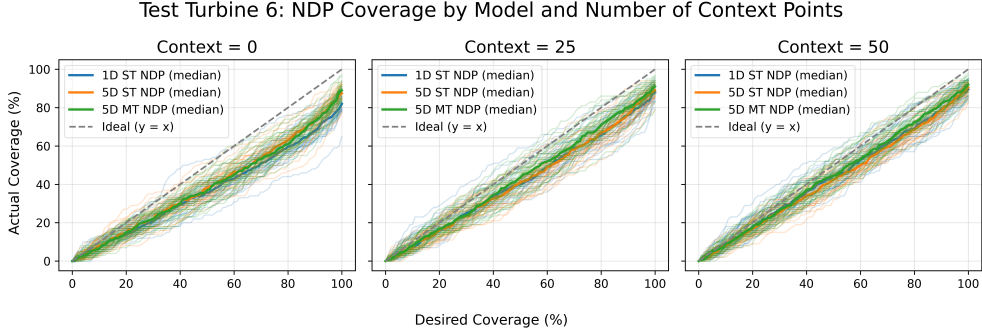


Fig. 7: Mean absolute error (MAE, left) and root mean squared error (RMSE, right) distributions for the one-dimensional single-task neural diffusion process (1D ST-NDP), five-dimensional single-task neural diffusion process (5D ST-NDP), and five-dimensional multi-task neural diffusion process (5D MT-NDP) on turbine 6 across context sizes 0, 25, and 50, aggregated over 30 test samples of 100 points each.

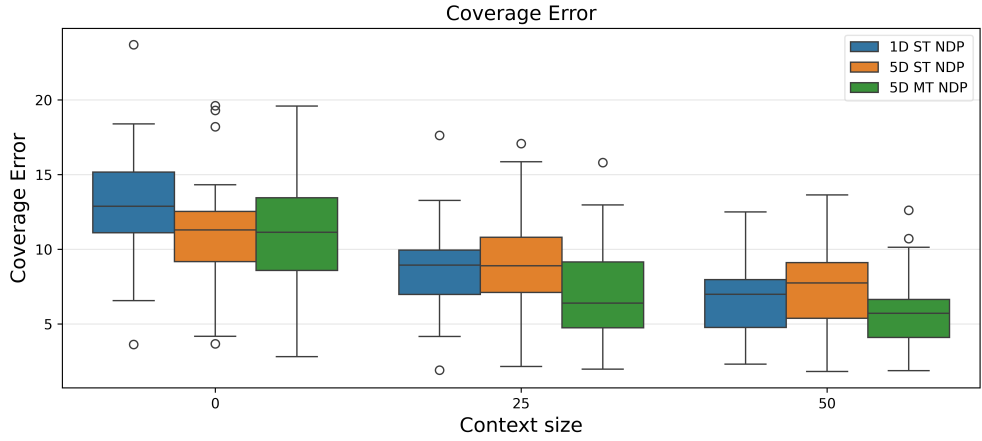
Fig. 8a compares empirical and nominal coverage for the same models. The five-dimensional MT-NDP demonstrates the best calibration overall, with coverage curves lying closest to the diagonal as context size increases. By contrast, the one-dimensional ST-NDP shows little benefit from context, underscoring its limited ability to capture multi-feature relationships. Finally, Fig. 8b summarises these findings using the CE. The five-dimensional MT-NDP again exhibits the strongest performance, achieving lower CE values than both the one-dimensional and five-dimensional ST-NDPs, particularly at higher context sizes. These results confirm that multi-task extension improves both point prediction accuracy and uncertainty calibration in a challenging case of turbine 6.

Table 1 reports quantitative results for turbine 6 across all models and context sizes. Several trends are evident. First, adding context points consistently improves both accuracy (MAE, RMSE) and calibration (CE) for all models, confirming the value of conditioning on task-specific data. Second, increasing the feature set from one to five dimensions reduces prediction error, with the five-dimensional ST-NDP outperforming its one-dimensional counterpart in most cases. Finally, the MT-NDP achieves the lowest errors overall: with 50 context points, it attains both the best point accuracy and the most well-calibrated uncertainty, reducing coverage error relative to the ST-NDP. These results demonstrate the advantage of the multi-task architecture



(a) Observed vs. nominal coverage.

Test Turbine 6: NDP Coverage Error by Model and Number of Context Points



(b) Coverage error distributions.

Fig. 8: Predictive uncertainty performance of the one-dimensional single-task neural diffusion process (1D ST-NDP), five-dimensional single-task neural diffusion process (5D ST-NDP), and five-dimensional multi-task neural diffusion process (5D MT-NDP) on turbine 6 across context sizes 0, 25, and 50, aggregated over 30 test samples of 100 points each. (a) Observed vs. nominal coverage. (b) Coverage error distributions.

in adapting to the distinct behaviour of turbine 6 and highlight its ability to perform few-shot inference.

6 Discussion

We examine the role of task conditioning in diffusion-based function models and its effect on generalisation and uncertainty estimation in multi-task regression. The results show that conditioning on limited context enables adaptation from a shared prior while preserving uncertainty calibration. Introducing a task encoder improves few-shot adaptation by enabling the model to distinguish tasks that deviate from the training

Table 1: Out-of-sample performance of single-task neural diffusion process (ST-NDP) and multi-task neural diffusion process (MT-NDP) models on turbine 6, averaged over 30 test functions (100 points each). Metrics reported: mean absolute error (MAE, kW), root mean squared error (RMSE, kW), and coverage error (CE, %). Bold values indicate the best overall performance across all models and context sizes. 1D: one-dimensional, 5D: five-dimensional.

Model	Context = 0			Context = 25			Context = 50		
	MAE	RMSE	CE	MAE	RMSE	CE	MAE	RMSE	CE
1D ST-NDP	66.539	90.491	13.052	56.641	77.766	8.779	53.283	73.429	6.865
5D ST-NDP	55.169	75.441	11.225	51.864	71.306	9.058	49.676	68.465	7.376
5D MT-NDP	55.291	75.974	11.375	49.183	67.805	6.986	47.268	65.636	5.691

distribution, while leaving the underlying diffusion process unchanged. This separation between diffusion-based function modelling and task encoding allows task-specific information to be incorporated without modifying the underlying generative process, preserving the probabilistic structure of the model. Several limitations point to directions for future research. The task encoder is deliberately simple and does not enforce full invariance; larger context budgets were not explored, and the experimental setting exhibits limited heterogeneity in some regimes. Addressing these aspects would clarify how architectural choices influence diffusion-based learning in multi-task settings.

7 Conclusion

We introduced MT-NDPs as a principled extension of diffusion-based function models that enable task-conditioned probabilistic regression. By augmenting NDPs with a lightweight task encoder, the proposed framework supports few-shot adaptation across related tasks while preserving calibrated uncertainty estimates. Empirical results on wind turbine SCADA data show that MT-NDPs consistently outperform single-task counterparts as context increases, particularly for tasks that deviate from the training distribution. These findings demonstrate that task structure can be incorporated into diffusion-based regression without altering the core diffusion mechanism, highlighting MT-NDPs as a flexible and scalable approach for multi-task learning in function space.

References

- [1] Sohl-Dickstein, J., Weiss, E., Maheswaranathan, N., Ganguli, S.: Deep unsupervised learning using nonequilibrium thermodynamics. In: International Conference on Machine Learning, pp. 2256–2265 (2015). PMLR
- [2] Ho, J., Jain, A., Abbeel, P.: Denoising diffusion probabilistic models. *Advances in neural information processing systems* **33**, 6840–6851 (2020)
- [3] Dutordoir, V., Saul, A., Ghahramani, Z., Simpson, F.: Neural diffusion processes. In: International Conference on Machine Learning, pp. 8990–9012 (2023). PMLR

- [4] Alvarez, M.A., Rosasco, L., Lawrence, N.D.: Kernels for vector-valued functions: A review. *Foundations and Trends® in Machine Learning* **4**(3), 195–266 (2012)
- [5] Wang, T., Hamann, A., Spittlehouse, D., Carroll, C.: Locally downscaled and spatially customizable climate data for historical and future periods for north america. *PloS one* **11**(6), 0156720 (2016)
- [6] Fiocchi, F., Ladopoulou, D., Dellaportas, P.: Probabilistic multilayer perceptrons for wind farm condition monitoring. *Wind Energy* **28**(4), 70012 (2025)
- [7] Hadjoudj, Y., Pandit, R.: A review on data-centric decision tools for offshore wind operation and maintenance activities: Challenges and opportunities. *Energy Science & Engineering* **11**(4), 1501–1515 (2023)
- [8] Chesterman, X., Verstraeten, T., Daems, P.-J., Nowé, A., Helsen, J.: Overview of normal behavior modeling approaches for scada-based wind turbine condition monitoring demonstrated on data from operational wind farms. *Wind Energy Science* **8**(6), 893–924 (2023)
- [9] Caruana, R.: Multitask learning. *Machine learning* **28**(1), 41–75 (1997)
- [10] Bonilla, E.V., Chai, K., Williams, C.: Multi-task gaussian process prediction. *Advances in neural information processing systems* **20** (2007)
- [11] Requeima, J., Tebbutt, W., Bruinsma, W., Turner, R.E.: The gaussian process autoregressive regression model (gpar). In: *The 22nd International Conference on Artificial Intelligence and Statistics*, pp. 1860–1869 (2019). PMLR
- [12] Williams, C.K., Rasmussen, C.E.: *Gaussian Processes for Machine Learning*. MIT press, Cambridge, MA (2006)
- [13] Garnelo, M., Rosenbaum, D., Maddison, C., Ramalho, T., Saxton, D., Shananhan, M., Teh, Y.W., Rezende, D., Eslami, S.A.: Conditional neural processes. In: *International Conference on Machine Learning*, pp. 1704–1713 (2018). PMLR
- [14] Kim, H., Mnih, A., Schwarz, J., Garnelo, M., Eslami, A., Rosenbaum, D., Vinyals, O., Teh, Y.W.: Attentive neural processes. *arXiv preprint arXiv:1901.05761* (2019)
- [15] Kim, D., Cho, S., Lee, W., Hong, S.: Multi-task neural processes. *arXiv preprint arXiv:2110.14953* (2021)
- [16] Maldonado-Correa, J., Martín-Martínez, S., Artigao, E., Gómez-Lázaro, E.: Using scada data for wind turbine condition monitoring: A systematic literature review. *Energies* **13**(12), 3132 (2020)
- [17] Ladopoulou, D., Hong, D.M., Dellaportas, P.: Probabilistic wind power modelling via heteroscedastic non-stationary gaussian processes. *Energy Reports* **15**, 108895

(2026)

- [18] Rogers, T., Gardner, P., Dervilis, N., Worden, K., Maguire, A., Papatheou, E., Cross, E.: Probabilistic modelling of wind turbine power curves with application of heteroscedastic gaussian process regression. *Renewable Energy* **148**, 1124–1136 (2020)
- [19] Pandit, R.K., Infield, D., Kolios, A.: Gaussian process power curve models incorporating wind turbine operational variables. *Energy Reports* **6**, 1658–1669 (2020)
- [20] Chen, N., Qian, Z., Nabney, I.T., Meng, X.: Wind power forecasts using gaussian processes and numerical weather prediction. *IEEE Transactions on Power Systems* **29**(2), 656–665 (2013)
- [21] Yu, Y., Han, X., Yang, M., Yang, J.: Probabilistic prediction of regional wind power based on spatiotemporal quantile regression. In: 2019 IEEE Industry Applications Society Annual Meeting, pp. 1–16 (2019). IEEE
- [22] Yu, Y., Yang, M., Han, X., Zhang, Y., Ye, P.: A regional wind power probabilistic forecast method based on deep quantile regression. *IEEE Transactions on Industry Applications* **57**(5), 4420–4427 (2021)
- [23] Zhou, Y., Sun, Y., Wang, S., Mahfoud, R.J., Alhelou, H.H., Hatziargyriou, N., Siano, P.: Performance improvement of very short-term prediction intervals for regional wind power based on composite conditional nonlinear quantile regression. *Journal of Modern Power Systems and Clean Energy* **10**(1), 60–70 (2021)
- [24] Zhang, H., Liu, Y., Yan, J., Han, S., Li, L., Long, Q.: Improved deep mixture density network for regional wind power probabilistic forecasting. *IEEE Transactions on Power Systems* **35**(4), 2549–2560 (2020)
- [25] Lugmayr, A., Danelljan, M., Romero, A., Yu, F., Timofte, R., Van Gool, L.: Repaint: Inpainting using denoising diffusion probabilistic models. In: Proceedings of the IEEE/CVF Conference on Computer Vision and Pattern Recognition, pp. 11461–11471 (2022)
- [26] Plumley, C.: Kelmarsh wind farm data (0.0. 3). Zenodo, February (2022)
- [27] Nichol, A.Q., Dhariwal, P.: Improved denoising diffusion probabilistic models. In: International Conference on Machine Learning, pp. 8162–8171 (2021). PMLR
- [28] Kingma, D.P., Ba, J.: Adam: A method for stochastic optimization. arXiv preprint arXiv:1412.6980 (2014)
- [29] Kolmogorov, A.N.: Foundations of the Theory of Probability: Second English Edition. Courier Dover Publications, NY, USA (2018)

Appendix A Gaussian Processes (GPs)

A GP $f : \mathbb{R}^D \rightarrow \mathbb{R}$ is a stochastic process such that, for any finite collection of inputs $X = \{x_i\}_{i=1}^N \subset \mathbb{R}^D$, the vector of function evaluations $f(X) = [f(x_1), \dots, f(x_N)]^T$ follows a multivariate normal distribution [12]. GPs satisfy the Kolmogorov extension theorem, which guarantees that all finite-dimensional marginals are mutually consistent under permutation and marginalisation [29]. This provides a principled Bayesian framework for modelling distributions over functions, enabling exact inference with predictive uncertainty. In our experiments presented in Section 5, we use GP regression as a benchmark model, so we briefly outline its formulation here.

In the regression setting, we are given a data vector $y = \{y_i\}_{i=1}^N \in \mathbb{R}^N$ whose entries are noisy evaluations of some function $f(\cdot)$ on a collection of D -dimensional vectors $X = \{x_i\}_{i=1}^N \in \mathbb{R}^{N \times D}$. Each y_i is assumed to be a noisy observation of $f(x_i)$, with independent Gaussian noise of mean 0 and variance σ^2 . Placing a GP prior over $f(\cdot)$, with mean function $\mu(\cdot)$ and covariance kernel $k_\theta(\cdot, \cdot)$, gives the joint distribution

$$f(X) \sim \mathcal{N}(\mu(X), K(X, X)), \quad (\text{A1})$$

where $\mu(X) = [\mu(x_1), \dots, \mu(x_N)]^T$ and $K(X, X)_{ij} = k_\theta(x_i, x_j)$ for all i, j .

The predictive distribution for future observations y^* with covariates X^* is Gaussian with mean and variance

$$E(y^*|y) = \mu(X^*) + K(X^*, X)A^{-1}(y - \mu(X)), \quad (\text{A2})$$

$$V(y^*|y) = K(X^*, X^*) - K(X^*, X)A^{-1}K(X, X^*). \quad (\text{A3})$$

For our experiments, we use the RBF kernel:

$$k_{\text{RBF}}(x_i, x_j|\theta) = \sigma_f^2 \exp\left(-\frac{1}{2} \sum_{d=1}^D \frac{(x_{i,d} - x_{j,d})^2}{\ell_d^2}\right), \quad (\text{A4})$$

where $\theta = \{\sigma_f^2, \ell_1, \ell_2, \dots, \ell_D\}$ are the kernel hyperparameters, with ℓ_d denoting the length-scale parameters and σ_f^2 representing the output variance.

While the RBF kernel is widely used and often effective in practice, encoding realistic prior assumptions through kernel design remains challenging, particularly for larger datasets and in higher-dimensional spaces. In addition, GPs assume Gaussian finite-dimensional marginals, restricting the class of functions they can represent. These issues motivate the exploration of alternative stochastic process models that relax Gaussianity while retaining uncertainty quantification and other desirable characteristics such as exchangeability.

Appendix B Diffusion probabilistic models (DPMs)

DPMs were introduced as a class of generative models inspired by non-equilibrium thermodynamics [1]. The central idea is to define a forward process, in which the structure of the data distribution is gradually destroyed by the iterative addition

of Gaussian noise, and a corresponding reverse process that learns to invert this corruption.

The de-noising diffusion probabilistic model (DDPM) [2] simplified and stabilised training and has become the standard formulation. Following [2, 3], the forward process begins from the input data distribution $q(s_0)$, where $s_0 \in \mathbb{R}^D$ denotes a D -dimensional data vector. It defines a fixed Markov chain over the sequence $s_{0:T} = \{s_0, \dots, s_T\}$ with density

$$q(s_{0:T}) = q(s_0) \prod_{t=1}^T q(s_t | s_{t-1}) \quad (\text{B5})$$

and conditional distributions

$$q(s_t | s_{t-1}) = \mathcal{N}\left(\sqrt{1 - \beta_t} s_{t-1}, \beta_t I_D\right), \quad (\text{B6})$$

where $\{\beta_t \in (0, 1)\}_{t=1}^T$ is a variance schedule controlling the magnitude of injected noise and I_D is the $D \times D$ identity matrix. After T steps, the distribution approaches Gaussian noise, $q(s_T) \approx \mathcal{N}(0, I)$. Early implementations used a linear variance schedule, while later work demonstrated that a cosine schedule improves performance by distributing noise more evenly across diffusion steps [27]. A variance schedule defines the cumulative noise parameter

$$\bar{\alpha}_t = \prod_{j=1}^t (1 - \beta_j), \quad (\text{B7})$$

which quantifies the retained signal at step t . In the cosine schedule,

$$\bar{\alpha}_t = \frac{f(t/T)}{f(0)}, \quad f(\lambda) = \cos^2\left(\frac{\pi}{2} \frac{\lambda+s}{1+s}\right), \quad (\text{B8})$$

where T is the total number of steps and s a small offset. This design avoids excessive noise at the beginning and end of the process, yielding more stable training and improved sample quality.

The reverse process is intractable in closed form, but can be approximated by a NN that predicts the injected noise. The mean of the reverse transition is parameterised as

$$\mu_\theta(s_t, t) = \frac{1}{\sqrt{\alpha_t}} \left(s_t - \frac{\beta_t}{\sqrt{1 - \bar{\alpha}_t}} \epsilon_\theta(s_t, t) \right), \quad (\text{B9})$$

where $\alpha_t = 1 - \beta_t$, $\bar{\alpha}_t = \prod_{j=1}^t \alpha_j$, and $\epsilon_\theta : \mathbb{R}^D \times \{1, \dots, T\} \rightarrow \mathbb{R}^D$ is a NN that predicts the injected noise vector. Training is carried out by minimising the score-matching loss

$$\mathbb{E}_{t, s_0, \epsilon} [\|\epsilon - \epsilon_\theta(s_t, t)\|^2], \quad (\text{B10})$$

where $s_t = \sqrt{\bar{\alpha}_t} s_0 + \sqrt{1 - \bar{\alpha}_t} \epsilon$ and $\epsilon \sim \mathcal{N}(0, I)$. Since $q(s_T) \approx \mathcal{N}(0, I)$, generating new samples requires only running the learned reverse process starting from Gaussian noise.

This framework enabled diffusion models to achieve state-of-the-art generative performance, rivalling generative adversarial networks (GANs) and autoregressive models. Building on DDPMs, Repaint [25] adapted the approach to image inpainting by conditioning on context points during the reverse process, without altering the pre-trained DDPM. This method achieved high-quality and diverse reconstructions under challenging conditions, outperforming autoregressive and GAN-based baselines.

In parallel, NPs were proposed as a stochastic process model combining NNs with an encoder–decoder architecture [13]. NPs learn to map a set of context points into a latent task representation, which is then used by a decoder to generate predictions at target inputs. This provides scalability and the ability to adapt to new tasks with only a few observations, but standard NPs often underfit and produce poorly calibrated uncertainty [14]. Latent and attentive variants improve correlations between targets, but still fall short of fully consistent Bayesian behaviour [3].

NDPs unify these two developments, drawing on diffusion-based generative modelling to overcome the Gaussian assumptions of NPs while retaining their scalability and adaptability. NDPs extend diffusion models from distributions over data to distributions over functions [3], thereby enabling uncertainty-aware regression.

Appendix C Dataset description

An operational status and events file was used to filter the SCADA data and ensure consistent modelling of normal turbine behaviour. These logs provide detailed information on turbine operating states, including technical failures as well as operational or environmental standbys and warnings. To enable accurate modelling, all data associated with out-of-control conditions were removed so that model training was based solely on stable operating periods. Specifically, records corresponding to standbys, warnings, and operational stops were excluded. In addition, data from the week preceding each forced outage was discarded to reduce the likelihood of capturing deteriorating states. The resulting data elimination process is also described and illustrated in [6].

Fig. C1a shows the wind speed–power curves for the six turbines after filtering. The curves are highly consistent and non-linear across wind turbines, with relatively few points observed at very high and very low wind speeds. These sparse regions are particularly challenging for probabilistic models such as GPs (see Section 5, Fig. 4). To examine directional effects, Fig. C1b presents the joint distribution of wind speed, wind direction, and power output for wind turbine 1. As expected, wind speed is the dominant component of variability. However, even at fixed wind speeds, power output varies with wind direction, likely reflecting terrain influences. Figure C2a presents mean nacelle temperature against mean power output. The pattern is more complex: rather than a monotonic trend, the relationship is approximately S-shaped. At intermediate power output, around 1000 kW, nacelle temperatures are on average lower than at low and high outputs. This non-linear behaviour highlights nacelle temperature as a particularly interesting covariate, since it reflects both operational load and thermal dynamics within the wind turbine. In Fig. C2b, we show the relationship between mean transformer temperature and mean power output across the six wind turbines. The curves are highly consistent, suggesting that transformer temperature

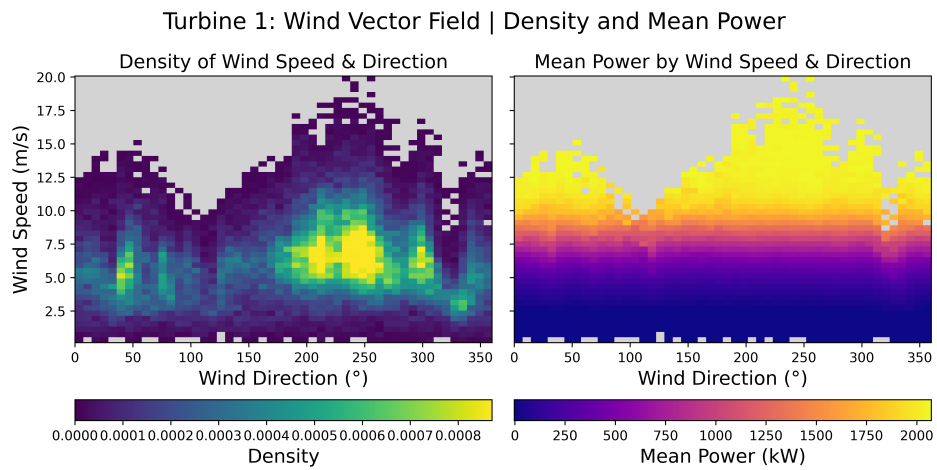
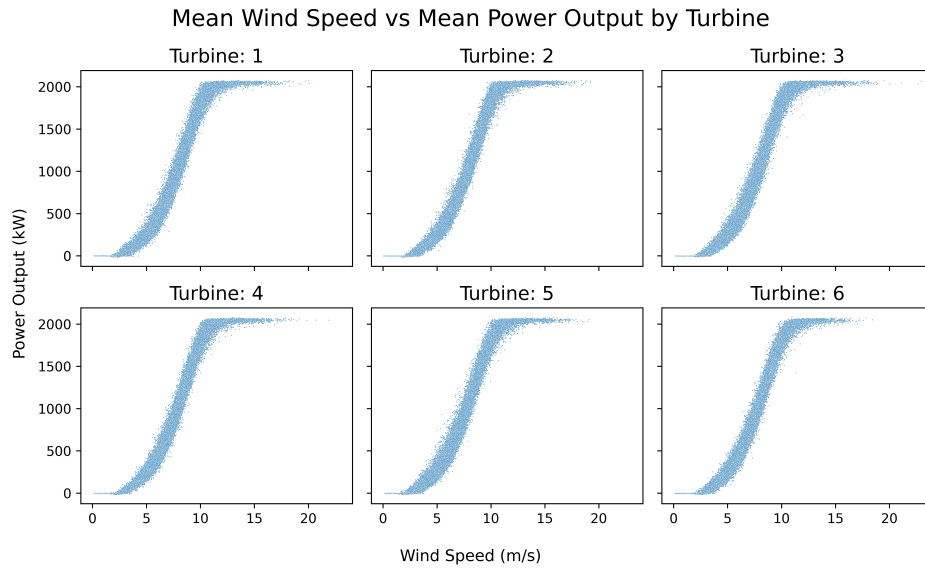


Fig. C1: SCADA data for the six turbines from the Kelmarsh wind farm [26] after removing standbys and warnings using the operational status and events file. (a) Wind power curves showing mean power output (kW) by mean wind speed (m/s). (b) Joint distribution of mean wind speed (m/s) and mean wind direction (°) for turbine 1 (left), and mean power output (kW) by mean wind speed (m/s) and wind direction (°) for turbine 1 (right).

scales predictably with power output and may provide additional explanatory power beyond wind speed.

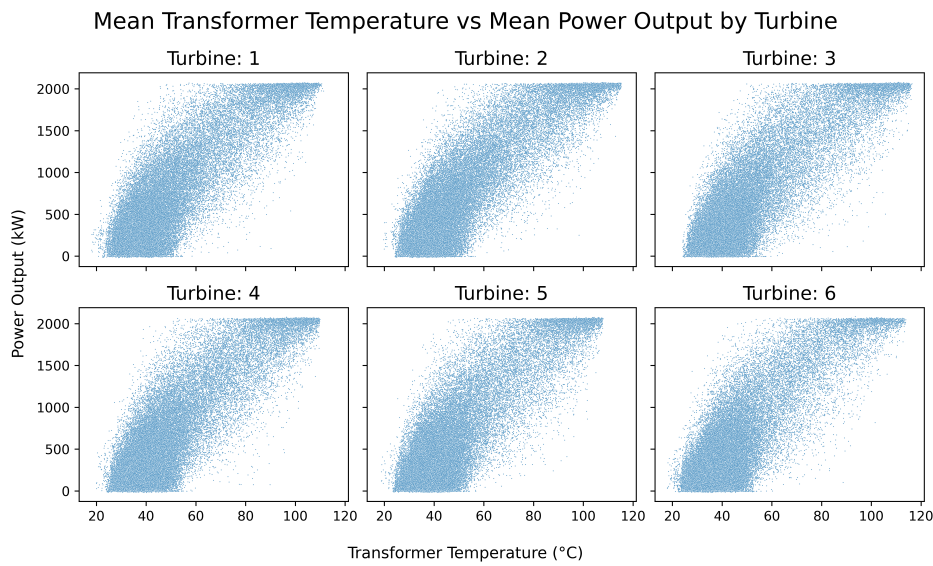
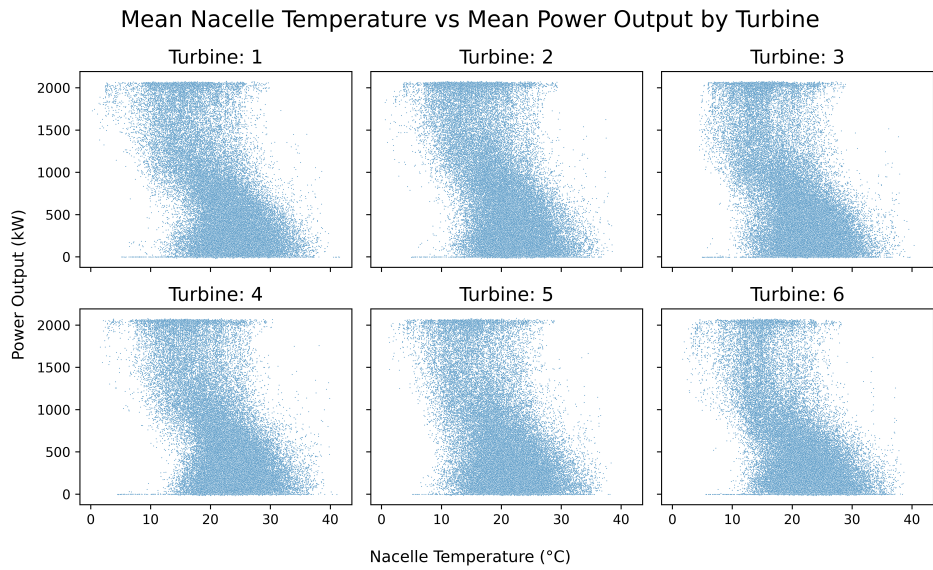


Fig. C2: SCADA data for the six turbines from the Kelmarsh wind farm [26] after removing standbys and warnings using the operational status and events file. (a) Mean power output (kW) by mean nacelle temperature (°C). (b) Mean power output (kW) by mean transformer temperature (°C).

Appendix D 1D NDP against 5D NDP

The five-dimensional NDP extends the one-dimensional baseline by incorporating additional input features: the cosine and sine of wind direction, transformer temperature, and nacelle temperature, alongside wind speed.

Test Turbine 1: 1D ST NDP vs 5D ST NDP Test Losses by Number of Context Points

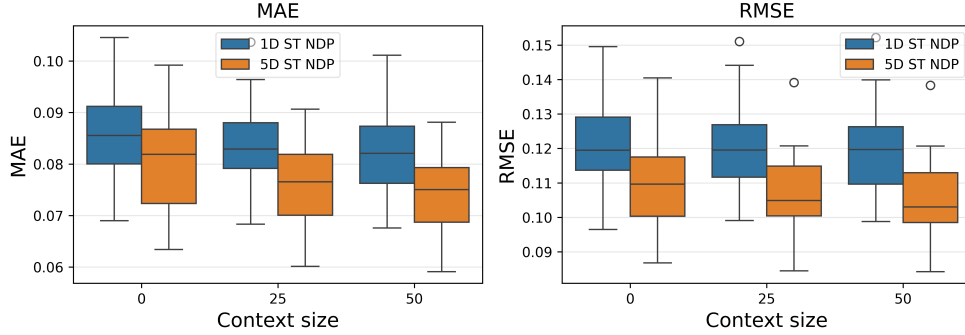


Fig. D3: Distributions of mean absolute error (MAE, left) and root mean square error (RMSE, right) for the one-dimensional (1D) and five-dimensional (5D) neural diffusion process (NDP) models, evaluated with 0, 25, and 50 context points. Results are aggregated over 30 test functions of 100 points each from turbine 1. ST: single-task.

Test Turbine 1: 1D ST NDP vs 5D ST NDP Coverage by Number of Context Points

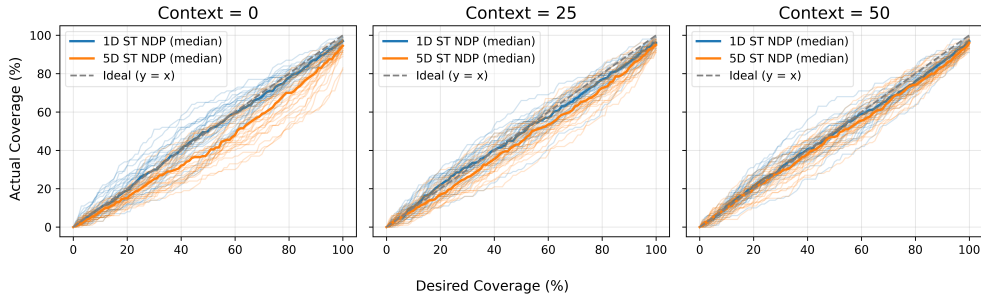


Fig. D4: Observed vs. theoretical coverage probabilities for the one-dimensional (1D) and five-dimensional (5D) neural diffusion process (NDP) models with 0, 25, and 50 context points. Results are averaged over 30 test functions of 100 points each from turbine 1. ST: single-task.

Fig. D3 compares the point prediction errors of the one-dimensional and five-dimensional NDP models across different context sizes. Incorporating more input features leads to a clear reduction in both MAE and RMSE, demonstrating the added explanatory power of the extended feature set. Notably, the benefit of context is much

more apparent in the five-dimensional NDP model, where performance improves consistently as context size increases. In contrast, the one-dimensional NDP model shows little to no improvement when additional context points are provided.

Test Turbine 1: 1D ST NDP vs 5D ST NDP Coverage Error by Number of Context Points

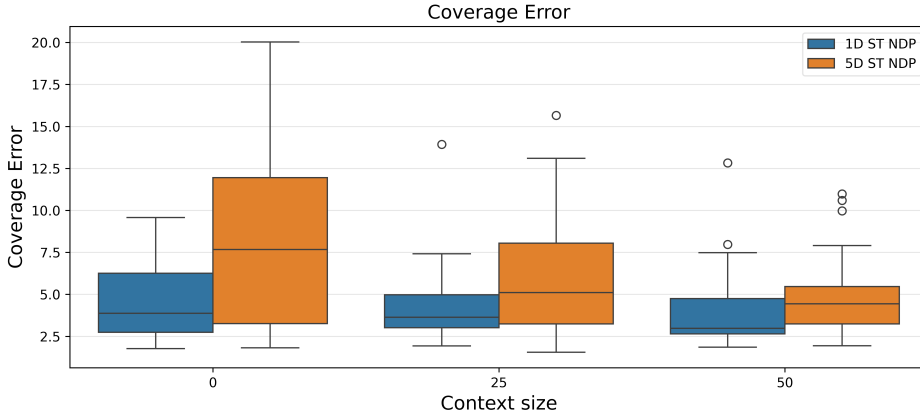


Fig. D5: Coverage error for the one-dimensional single-task neural diffusion process (1D ST NDP) and five-dimensional single-task neural diffusion process (5D ST NDP) models with 0, 25, and 50 context points. Results are computed over 30 test functions of 100 points each from turbine 1.

Fig. D4 presents observed versus nominal coverage for both models at different context sizes. The five-dimensional NDP shows steady improvement in calibration with increasing context, whereas the one-dimensional NDP remains largely unaffected by context size. Interestingly, the one-dimensional NDP achieves slightly better coverage alignment than the five-dimensional NDP when both are provided with 50 context points. This raises the question of whether the five-dimensional NDP model would outperform the one-dimensional model given a larger context set, a question left open here due to computational constraints.

Finally, Fig. D5 summarises coverage performance using the CE metric. The results confirm that context improves calibration for the five-dimensional NDP, narrowing the gap to the one-dimensional NDP model. When considered alongside the substantial accuracy gains in Fig. D3, the evidence suggests that the five-dimensional NDP provides a meaningful improvement over the one-dimensional NDP baseline, particularly in balancing accuracy with uncertainty calibration.

Table D1 provides a quantitative summary of the comparisons, aggregating point prediction accuracy (MAE, RMSE) and predictive uncertainty calibration (CE) across all models and context sizes for turbine 1. The results confirm the visual trends: while the GP achieves similar MAE and RMSE to the NDP, it performs very poorly in terms of uncertainty calibration, with a coverage error more than four times higher. Among the NDP variants, incorporating additional features (from one-dimensional to

Table D1: Out-of-sample performance of Gaussian process (GP) and single-task neural diffusion process (ST-NDP) models on turbine 1, averaged over 30 test functions (100 points each). Metrics reported: mean absolute error (MAE, kW), root mean squared error (RMSE, kW), and coverage error (CE, %). 1D: one-dimensional, 3D: three-dimensional, 5D: five-dimensional.

<i>Model</i>	Context = 0			Context = 25			Context = 50		
	MAE	RMSE	CE	MAE	RMSE	CE	MAE	RMSE	CE
1D GP	51.636	75.596	18.075	–	–	–	–	–	–
1D ST-NDP	52.603	75.139	4.584	51.273	74.568	4.181	50.545	74.137	3.938
3D ST-NDP	60.967	88.096	9.731	52.338	74.312	6.750	50.855	73.537	5.369
5D ST-NDP	49.429	67.685	8.351	46.962	66.007	6.029	45.791	65.301	4.816

five-dimensional) consistently reduces prediction error, while increasing the number of context points improves both accuracy and calibration.